International Journal of Scientific Engineering and Technology (ISSN : 2277-1581)
Volume No.2, Issue No.9, pp : 825-829 1 Sept. 2013

Cell Based Deformation Calculation for Porous Material

Yi Xiao, Qing-Hua Qin
Research School of Engineering,
Australian National University, Canberra, ACT 2601, Australia
yi.xiao@anu.edu.au, qinghua.qin@anu.edu.au

Abstract— ***This paper deals with the calculation of full-field displacement over a surface of metallic foam. Owing to the failure of traditional displacement measurement method which calculates the correlation of intensity pattern between two regions, we propose a cellular based full field displacement calculation. The nodes are extracted from the cell boundary and nodal displacement is found by a thin plate spline based robust point matching. The proposed approach involves multiple-step image processing including cell region segmentation, cell region matching and nodal matching. As a result, the displacement at a given node can be found. Metallic foam is used for assessing the effectiveness and accuracy of the proposed algorithm. The results show that local displacements around cell boundaries on the surfaces of the specimen can be effectively determined with the proposed method, thus it appears that the method is promising for predicting displacements of complex cellular solids.***

Keywords— cellular material, cell-based approach, foam, DIC.

1. Introduction

Metallic foams are of light-weight and high strength in shear/compression [1]. Researchers have been endeavored in understanding relationships between the morphology and the properties of metallic foams in order to effectively exploit these properties in engineering design. On the other hand, a number of methods for calculating optical full-field of displacement/strain and then identifying effective material properties has been recently proposed for analyzing performance of various engineering materials [2-7]. Among these methods, the digital imaging correlation (DIC) has become increasingly popular in the past two decades due to its relatively simple principle and flexibility in its adjustable scales from micro to nanoscale [2,8,9]. With the DIC method, the nodal displacement on the surface of a planar specimen is obtained by comparing correlatively a pair of digital images taken before and after the imposed deformation of the specimen [10]. In the past decades, various subset-based DIC methods [11] have been developed, which can be viewed as the main streams in DIC technique. These methods find the displacement of a point (node) cantered at a subset by searching the maximal correlation coefficient that is determined by examining the intensity pattern of the subset with the intensity pattern of subsets in the deformed image.

An inherent limitation of the subset-based DIC method is that the choice of the subset size must compromise between correlation accuracy, interpolation error and computational cost. For interpolation, the amount of interpolated pixels accounted to estimated shape function is affected by the subset size, and hence the accuracy can be affected. Some problems of optimal subset size selection for a specimen with a continuous area have been addressed in a number of studies [12]. As for materials containing discontinuous areas such as pores, inclusions or cracks, the choice of subset size is much difficult. Special treatments must be taken either to define the subset within the continuous region or to handle the discontinuity across the interface of two distinct areas (phases). These strategies have only been applied to testing specimens with simple geometries containing a single hole [13] or a single crack [14].

The so-called extended digital image correlation (X-DIC) had been used by many researchers [15] to handle problems of a specimen with sparse distributed discontinuities, due to its excellent shape adaptability and smooth ability. The X-DIC discretizes an image area into some finite elements (segments) which are linked by nodes. Unlike in the original subset based DIC methods where the displacements are found point by point, all the nodal values in the X-DIC approach are correlated simultaneously by various matching algorithms. The full field displacement can be obtained via interpolation using the nodal values or finite element smoothing [16-18].

Current displacement field calculations with both original DIC and X-DIC are pixel-based, where intensity patterns in images are compared via correlation metrics. The performance of both DIC and X-DIC still relies on the subset size and the texture pattern of pixel's intensity in the subset. For a cellular solid, its surface is dominant with holes and its cell walls are relatively thin. The subset size in cell wall regions can only be very small that it is inefficient to spatially characterize the intensity pattern in such a subset area, dampening the displacement field calculation performance using original subset-based or X-DIC methods.

In this study, we develop a new cellular-based method aiming at retrieving displacement results of metallic foams. The displacement field on the surface of a metallic foam is obtained from the interpolation on the known nodal values. In the process of nodal displacement calculation, a set of nodes from a reference cell and the corresponding node set of the deformed cell are matched by a TPS-RPM method, which was originally developed in computer vision and pattern recognition [19] for image registration and shape matching. The proposed nodal value calculating involves a multiple-step image processing to locate cell boundaries from raster images and establish mapping between nodes before and after deformation.

2. Procedure of Displacement field calculation

The proposed approach for displacement field calculation involves a series of image processing techniques, including cell region segmentation, cell region matching and cell boundary point matching.

Image segmentation is used to locate cell regions and their boundaries in an image of a surface of metallic foam. The open space which has a lower illumination is separated from cell walls which have a considerably higher illumination via a thresholding process. During the process, individual pixels in the image are marked as "cell" pixels (with a value of '1') if their value is less than a threshold value and as 'open space' pixels (with a value of '0') otherwise. The key to have the regions segmented exactly along the cell boundaries is the choice of the threshold value. In our analysis, trial-and-error is used to determine the threshold value.

A binary image containing many blobs (or regions) is created after the thresholding process. A blob is a cell region consisting a series of connected 'cell' pixel with the value of '1'. Specks (small blobs) may be generated during the process of binarizing and can be removed by checking the number of pixels in a blob.

In this study, matching a reference cell region to its deformed cell region is a problem of having a region in an image and finding its closet match among a set of regions in another image. A so called maximum-overlapping-area criterion is proposed for processing cell region matching: let R_k be the region of cell k in the reference image and R' be the corresponding region of cell k in the deformed image. R' is identified by

$$S(R_k, R') = \max\{S(R_k, R'_i)|_{i=1,2,...n}\} \quad (1)$$

Here $S(R_k, R'_i)$ is the number of pixels in the intersecting area of the two regions R'_i and R_k, n is the total number of cell regions in the deformed image. The criterion is based on the fact that cell regions in the image of the compressed specimen deform in shape but have small change in locations (i.e. the small displacement problem).

In the proposed approach, boundary points in a cell region are extracted as nodes. The nodes in a reference cell are matched to their corresponding nodes in the deformed cell by a TPS-RPM. The detail procedure of the TPS-RPM used for node matching is described in next section. Nodal displacements are calculated from the pairs of matched nodes. Displacements at any point in the open space bound by cell boundaries are then found by the natural neighbour interpolation (http://en.wikipedia.org/wiki/Natural_neighbor). The interpolation of displacements is based on the method of Delaunay triangulations [20]. It is superior to other interpolation methods in obtaining a continuous surface when the distribution of the data is anisotropic or data density varies.

3. TPS-RPM for node matching

Consider two point sets, $\mathbf{X} = \{\mathbf{x}_i : i = 1, 2, ..., N_1\}$ along the reference cell boundary and $\mathbf{Y} = \{\mathbf{y}_j : j = 1, 2, ..., N_2\}$ along the deformed cell's boundary, we apply TPS-RPM to determine the correspondence between $\mathbf{X}$ and $\mathbf{Y}$ and match them accordingly [19]. According to Ref. [19], the following energy function can be minimized in the form:

$$E(\mathbf{M}, f) = \sum_{j=1}^{N_2}\sum_{i=1}^{N_1} m_{ij} \| \mathbf{y}_i - f(\mathbf{x}_i) \|^2 + \lambda \| Lf \|^2 + T\sum_{j=1}^{N_2}\sum_{i=1}^{N_1} m_{ij} \log m_{ij} - \zeta \sum_{j=1}^{N_2}\sum_{i=1}^{N_1} m_{ij} \quad (2)$$

which subjects to the following constraints,

$$\begin{cases} 0 \le m_{ij} \le 1 \quad \text{for } i = 1, 2, ..., N_1 + 1;\ j = 1, 2, ..., N_2 + 1 \\ \sum_{j=1}^{N_2+1} m_{ij} = 1 \quad \text{for } i = 1, 2, ..., N_1 \\ \sum_{i=1}^{N_1+1} m_{ij} = 1 \quad \text{for } j = 1, 2, ..., N_2 \end{cases} \quad (3)$$

where the matrix characterize the correspondence between and as follows

$$\mathbf{M} = \begin{pmatrix} m_{11} & \cdots & m_{1,N_2} & m_{1,N_2+1} \\ \vdots & \ddots & \vdots & \vdots \\ m_{N_1,1} & \cdots & m_{N_1,N_2} & m_{N_1,N_2+1} \\ m_{N_1+1,1} & \cdots & m_{N_1+1,N_2} & 0 \end{pmatrix} \quad (4)$$

It consists of two parts. The $N_1 \times N_2$ inner sub-matrix defines the correspondence between $\mathbf{X}$ and $\mathbf{Y}$. If $\mathbf{x}_i$ corresponds to $\mathbf{y}_j$, then $m_{ij} = 1$, otherwise $m_{ij} = 0$. The $(N_2+1)_{th}$ column and the $(N_1+1)_{th}$ row define the outliers in $\mathbf{X}$ and $\mathbf{Y}$, respectively. If $\mathbf{x}_i$ (or $\mathbf{y}_j$) is an outlier, then $m_{i,N_2+1} = 1$ (or $m_{N_1+1,j} = 1$). f in Eq. 2 denotes non-rigid spatial transform between $\mathbf{X}$ and $\mathbf{Y}$, with the form of $f(\mathbf{x}_i) = \mathbf{x}_i \cdot \mathbf{a} + \mathbf{k}(\mathbf{x}_i) \cdot \mathbf{w}$, in which $\mathbf{a}$ is a 3×3 matrix representing the affine transform and $\mathbf{w}$ is a $N_1 \times 3$ matrix representing the non-affine warping transform. $\mathbf{k}_j(\mathbf{x}_i)$ is a kernel for TPS. In this study, $\mathbf{k}_j(\mathbf{x}_i) = \| \mathbf{x}_j - \mathbf{x}_i \|^2 \log \| \mathbf{x}_j - \mathbf{x}_i \|$, for $i = 1, 2, ..., N_1$; $j = 1, 2, ..., N_2 + 1$.

Under the mapping f, the point set $\mathbf{X}$ is transformed to $\mathbf{X}' = \{\mathbf{x}'_i : i = 1, 2, ..., N_1\}$. The first term in Eq. 1 is a linear assignment- least square energy measurement, L in the second term is an operator denoting the smoothness regularization of f, with

$$\| Lf \|^2 = \iint [(\frac{\partial^2 f}{\partial u^2})^2 + 2(\frac{\partial^2 f}{\partial u \partial v})^2 + (\frac{\partial^2 f}{\partial v^2})^2] du dv \quad (5)$$

where u and v represent the two coordinates of the points. The entropy term (the third term) in Eq. 1 is to control the fuzziness of the energy function in the deterministic annealing process. T is called the temperature parameter, which decreases gradually during the process. The last term in Eq. 1 is designed to prevent excessive outlier rejection. λ and ζ are the weighting parameters to balance these terms.

The TPS-RPM algorithm is featured with a two-step up-date process: update the correspondences by differentiating the

energy function in Eq. 1 with respect to $\mathbf{M}$, and setting the result to zero; update the transformation by the least-squares approach to solve for the TPS parameters. The update process is controlled by the annealing scheme. According to a linear annealing rate r ($r<1$), The temperature T is reduced with $T_{t+1}=T_t \cdot r$, starting from $T_0=T_{initial}$. Repeat the two-step updates till the object function convergence at a final temperature T_{final}.

4. Assessment and discussion

To test the feasibility and efficiency of the proposed algorithm, an example of a metallic foam specimen is considered. The in-plane displacements of these cellular structures are calculated using the proposed algorithm.

4.1 Parameter setting and point matching performance

In the process of point matching, the choice of initial value of $T_{initial}$ is critical. When $T_{initial}$ is too large, the point matching algorithm may be time consuming. When $T_{initial}$ is too small, the algorithm may fail to converge to an optimal solution. To guarantee the point matching reaches a global optimal solution and keeps low computational cost, $T_{initial}$ is set up as 10000 in our analysis, which is a value related to the largest squared distance of all point pairs. The temperature T is gradually reduced at an annealing rate of $r=0.53$, which is a value trading off the speed of annealing procedure and accuracy of the point matching.

Due to the presence of outliers and perturbations along the boundaries, it is not always desirable for the TPS-RPM algorithm to obtain binary one-to-one correspondence between two point sets with T approaching zero [19]. And when T is too small, the affine mapping may have the risk of flip. The annealing process stops at a minimum value of T (T_{final}) to avoid the flip of mapping. At T_{final}, most elements of matrix $\mathbf{M}$ are close, although not equal, to values 0 or 1. And taking the points with the most significant m_{ij} as matched points, the algorithm achieves satisfied point matching result.

Since the initial values of elements in $\mathbf{M}$ do not affect the elements' final values within [$T_{initial}$, T_{final}], we set all initial entries of $\mathbf{M}$ as $1/N_1$, and the outlier row and column are equal to $1/100N_1$. The initial values of $\mathbf{a}$ and $\mathbf{w}$ are $\mathbf{a}=\mathbf{I}$ and $\mathbf{w}=0$, where I is an identity matrix. $\mathbf{M}$, $\mathbf{a}$ and $\mathbf{w}$ are updated iteratively as T decreased.

The accuracy of the proposed displacement calculation depends on the performance of the point matching. In our assessment, the TPS-RPM algorithm rapidly brings two cell boundaries closer in space and more similar in shape from the initial iterations of the deterministic annealing procedure.

This assessment shows that the setting of final temperature T_{final} is deformation dependent. For the pairs of cell point sets that have small deformation, good matching is achieved at final iteration, and the sequential ordering of points is preserved. For some pairs of cell boundaries that are significantly deformed, when T is too small, the affine transform flipped, causing some points in a cell boundary map to points far away from their corresponding points in its deformed cell boundary and the sequential ordering of points is broken. Under our setting ($T_{final}=500$), the algorithm achieves satisfied point matching result. Only a few mismatches are introduced at the points in highly folded curves, but sequential ordering of points is preserved.

4.2 Numerical results for a designed specimen of metallic foams

An image (Fig. 1 (a)) of a designed dog-bone specimen of metallic foams is obtained from [21]. The specimen has at least one complete cell located at the center of effective test zone. It was sectioned by electro-discharge machining to avoid local damage to the cell walls. For quantitative measurement of the accuracy of point matching, a simulated synthetic image (Fig. 1 (b)) is generated. It is a shear transform ($f_s:(x,y)\rightarrow(x',y')$) on the image of Fig. 1(a). f_s is the shearing parallel to the y axis, in the transformation form of

$$x' = x, \quad y' = y + kx \tag{6}$$

Most nodes (cell boundary points) in Fig. 1(a) match their correspondences in Fig. 1(b); a number of points mismatch to the points a few pixels away from their correspondences.

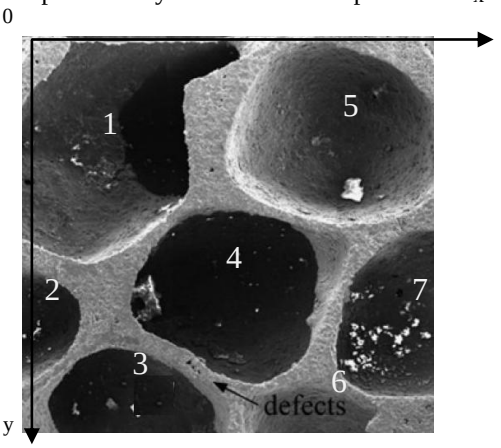

(a) Original image

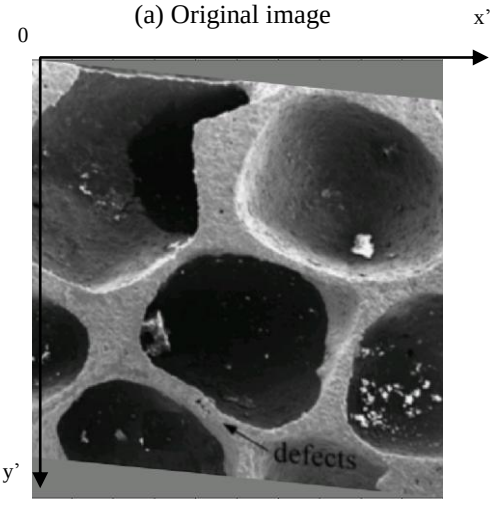

(b)Synthetic image transformed from that shown in Fig. 1 (a)

Fig. 1 A specimen of metallic foam

For a given point P, the relative deviation between the mapped point of P obtained by TPS-RPM and the point of P's

shear transform is used for the point matching evaluation as follows:

$$D = \left| \frac{u_y - u_y'}{u_y} \right| \quad (7)$$

where u_y is the displacement in y direction obtained from the shear transform shown in Eq. 13; u_y' is the displacement in y direction calculated by the proposed method.

Fig. 2 depicts the average relative deviations and theoretical dispalcment of point pairs in *y* direction for the 4th cell shown in Fig. 1(a), where the shear element $k = \{0.01, 0.03, 0.05, 0.1, 0.2, 0.3\}$, corresponding to the maximum displacements $d_m(\text{pixel}) = \{3, 9, 15, 30, 60, 89\}$ respectively. All the average relative deviations are between 2%~5% in *y* direction. Unlike the honeycomb, the average relative diviation values for the matelic foam increase with the increase of *k* as the number of mismatched point pairs increases greatly with the increase of *k*, causing the increasing of the average diviation value faster than the increasing of average displacement.

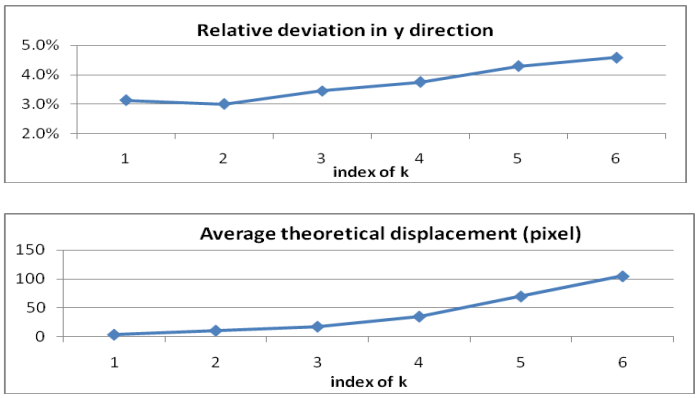

Fig. 2 The average relative deviation and theoretical displacement of the ordered points at different for the cell shown in Fig 1 (1 pixel = 0.03mm).

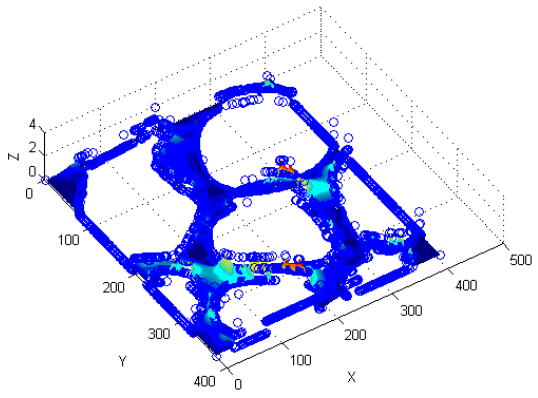

(a) Displacement in x direction

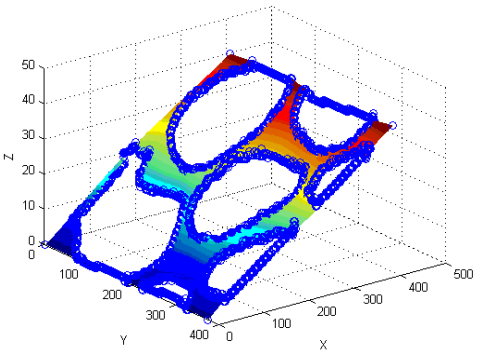

(b) Displacement in y direction

Fig. 3 Displacement of the metallic foam in x and y direction (1 pixel = 0.03mm).

Figs. 3(a) and (b) presents the substrate displacement fields in x and y directions obtained by the proposed algorithm for the metallic foam between the original and the sheared image. The reference point is at (0,0) in both images (Figs. 1(a) and (b)). The ground true of displacement is a shear represented in Eq. 6. The results from the proposed method are the displacement in y direction changing linearly with respect to x; displacement in x direction for most regions is less than 1 pixel. Large displacement occurs in sparse areas where the point pairs are mismatched.

5. Conclusion

The shape information of cells is used in this study for the full field displacement measurement of metallic foam. The displacement of any point in the cell wall region is obtained from the interpolation of nodal values. The nodes are extracted from the cell boundary points obtained after image segmentation. The nodal displacement values are found through a TPS-RPM method from the node sets before and after deformation

The accuracy of the proposed method for displacement measurement is mainly determined by the performance of point matching, which is quantitatively measured by the relative deviation of displacement between the mapped points obtained by TPS-RPM and the true deformed points in a shear transform with different from 0.01 to 0.3. The assessment shows that for a cell with complex geometry shape in the metallic foam, the number of mismatched point pairs is relatively larger (than that of honeycomb) and this number increases more significantly with the increase of k when k > 0.01. The average relative deviation is between 2%~5% and it is monotonically increasing with respect to k when k > 0.01.The results indicate that local displacements around holes' boundaries of a material's surface can be effectively determined with the proposed method under elastic deformation and it appears that the proposed method is promising for predicting displacements of complex cellular solids.

References

[1] L.J. Gibson and M.F. Ashby, Cellular solids: structure and properties, Cambridge: Cambridge University Press (1999)
[2] H. Haddadi and S. Belhabib, Use of rigid-body motion for the investigation and estimation of the measurement errors related to digital image correlation technique, Optics and Lasers in Eng, Vol. 46 (2008), 185-196
[3] Q.H. Qin, Y.W. Mai and S.W. Yu, Effective moduli for thermopiezoelectric materials with microcracks, International Journal of Fracture, Vol. 91 (1998), 359-371
[4] Q.H. Qin and M.V. Swain: Biomaterials, Vol. 25 (2004), 5081-5090
[5] Q.H. Qin and S.W. Yu, Effective moduli of thermopiezoelectric material with microcavities, International Journal of Solids and Structures, Vol. 35 (1998), 5085-5095
[6] X.Q. Feng, Y.W. Mai and Q.H. Qin, A micromechanical model for interpenetrating multiphase composites, Computational Materials Science, Vol. 28 (2003), 486-493
[7] Q.H. Qin, Material properties of piezoelectric composites by BEM and homogenization method, Composite Structures, Vol. 66 (2004) 295-299
[8] Z.F. Zhang, Y.L. Kang, H.W. Wang, Q.H. Qin, Y. Qiu, X.Q. Li, A novel coarse-fine search scheme for digital image correlation method, Measurement, Vol. 39 (2006), 710-718
[9] Y.L. Kang, Z.F. Zhang, H.W. Wang, Q.H. Qin, Experimental investigations of the effect of thickness on fracture toughness of metallic foils, Materials Science and Engineering: A 394(1), (2005), 312-319
[10] C. Su and L. Anand: http://dspace.mit.edu/handle/1721.1/3749 (visited 10 Aug 2012)
[11] J. Zhang, Y.X. Cai, W.J. Ye and T.X. Yu, On the use of the digital image correlation method for heterogeneous deformation measurement of porous solids, Optics and Lasers in Eng, Vol. 49 (2011), 200-209
[12] Y. Sun and J.H.L. Pang, Study of optimal subset size in digital image correlation of speckle pattern images Optics and Lasers in Eng, Vol. 45 (2007), 967-974
[13] A.R. Hamilton, N.R. Sottos and S.R. White, Local Strain Concentrations in a Microvascular Network, Experimental Mechanics,Vol. 50 (2010), 255-263
[14] J. Abanto-Bueno and J. Lambros, Investigation of crack growth in functionally graded materials using digital image correlation, Engineering Fracture Mechanics, Vol. 69 (2002), 1695-1711
[15] J. Rethore, F. Hild and S. Roux, Extended digital image correlation with crack shape optimization, International Journal for Numerical Methods in Engineering, Vol. 73 (2008), 248-272
[16],Y.F. Sun, J.H.L. Pang, C.K. Wong, F. Su, Finite element formulation for a digital image correlation method, Applied Optics, Vol. 44 (2005), 7357-7363
[17] Q. H. Qin and C. Mao, Coupled torsional-flexural vibration of shafts in mechanical engineering--I: finite element model, Computers & Structures, Vol. 58, 835-843, 1996
[18] Q. S. Yang, Q. H. Qin, L. H. Ma, X. Z. Lu, C. Q. Cui, A theoretical model and finite element formulation for coupled thermo-electro-chemo-mechanical media, Mechanics of Materials Vol. 42 (2010), 148-156
[19] H.L. Chui and A. Rangarajan, A new point matching algorithm for non-rigid registration, Computer Vision & Image Understanding, Vol. 89 (2003), 114-141
[20] Y. Xiao and H. Yan, Text region extraction in a document image based on the Delaunay tessellation, Pattern Recognition, Vol. 36 (2003), 799-809
[21] H.W. Song, Q.J. He, J.J. Xie and A. Tobota, Fracture mechanisms and size effects of brittle metallic foams: In situ compression tests inside SEM, Composites Science and Technology, Vol. 68 (2008), 2441-2450